

May be used only for educational or research purposes.

Citation:

Dong, Jiahao et al. "Giant and Controllable Photoplasticity and Photoelasticity in Compound Semiconductors." Phys. Rev. Lett. 129, no. 6 (3 August 2022).

<https://doi.org/10.1103/PhysRevLett.129.065501>.

Access to this work was provided by the University of Maryland, Baltimore County (UMBC) ScholarWorks@UMBC digital repository on the Maryland Shared Open Access (MD-SOAR) platform.

Please provide feedback

Please support the ScholarWorks@UMBC repository by emailing scholarworks-group@umbc.edu and telling us what having access to this work means to you and why it's important to you. Thank you.

Giant and Controllable Photoplasticity and Photoelasticity in Compound Semiconductors

Jiahao Dong,^{1,*} Yifei Li^{1,*} Yuying Zhou^{1,2} Alan Schwartzman¹ Haowei Xu,³ Bilal Azhar,¹
Joseph Bennett⁴ Ju Li^{1,3} and R. Jaramillo^{1,†}

¹*Department of Materials Science and Engineering, Massachusetts Institute of Technology, Cambridge, Massachusetts 02139, USA*

²*Shanghai Institute of Applied Physics, Chinese Academy of Sciences, Shanghai, 201800 China*

³*Department of Nuclear Science and Engineering, Massachusetts Institute of Technology, Cambridge, Massachusetts 02139, USA*

⁴*Department of Chemistry and Biochemistry, University of Maryland Baltimore County, Baltimore, Maryland 21250, USA*



(Received 5 November 2021; accepted 26 June 2022; published 3 August 2022)

We show that the wide-band gap compound semiconductors ZnO, ZnS, and CdS feature large photoplastic and photoelastic effects that are mediated by point defects. We measure the mechanical properties of ceramics and single crystals using nanoindentation, and we find that elasticity and plasticity vary strongly with moderate illumination. For instance, the elastic stiffness of ZnO can increase by greater than 40% due to blue illumination of intensity 1.4 mW/cm². Above-band-gap illumination (e.g., uv light) has the strongest effect, and the relative effect of subband gap illumination varies between samples—a clear sign of defect-mediated processes. We show giant optomechanical effects can be tuned by materials processing, and that processing dependence can be understood within a framework of point defect equilibrium. The photoplastic effect can be understood by a long-established theory of charged dislocation motion. The photoelastic effect requires a new theoretical framework which we present using density functional theory to study the effect of point defect ionization on local lattice structure and elastic tensors. Our results update the longstanding but lesser-studied field of semiconductor optomechanics, and suggest interesting applications.

DOI: [10.1103/PhysRevLett.129.065501](https://doi.org/10.1103/PhysRevLett.129.065501)

Introduction.—The literature on the interaction between light and the mechanical properties of semiconductors covers two distinct phenomena that have been more-or-less understood for decades: photostriction and photoplasticity. Photostriction occurs as illumination promotes electrons from the valence to the conduction band, thereby changing the cohesive energy and free volume of the crystal [1]. Photostriction can be calculated from thermodynamic coefficients, and typically has a small effect on the elastic modulus, although large effects have been reported [2,3]. Photoplasticity occurs as illumination changes the charge state of dislocations and point defects, thereby changing the force required for plastic deformation [4–9]. Photoplasticity is correlated with photoconductivity because deep levels that “store” charge, leading to persistent photoconductivity, can also contribute to dislocation pinning [4,6,10]. Giant photoplasticity has been reported in II–VI semiconductors; the magnitude of the photoplastic effect was brought into striking relief by a recent study of ZnS by Oshima *et al.* [11–15].

Large effects of illumination on elasticity—here termed *giant photoelasticity*—are less understood. Partially reversible elastic constant changes of up to 20% were reported in chalcogenide glasses and ascribed to photoinduced bond rearrangements [16,17]. Giant, reversible photoelasticity was reported based on nanoindentation measurements of ZnO and ZnS nanostructures and ascribed to surface

photovoltage (SPV), and it is recognized that SPV can generate optomechanical response in polar crystals via the piezoelectric effect [2,13,17,18]. It is also well-known that illumination can toggle between bistable lattice configurations at deep levels, such as DX centers in III–V's, and negative-*U* centers in oxides and chalcogenides [19–23]. The connections between point defects, deep level ionization, local lattice distortion, illumination, and elasticity have yet to be studied.

Here we report giant and reversible photoplasticity and photoelasticity in CdS, ZnS, and ZnO. We measure optomechanical effects using nanoindentation combined with light illumination of variable intensity and wavelength. We find that optomechanical response can be tuned by sample processing, guided by principles of defect engineering. We use density functional theory (DFT) to study the effect of deep level ionization on elasticity, and we find a diversity of large effects that are semiquantitatively consistent with our experimental results. Our results illustrate the atomic origins of large optomechanical effects that remain little studied, but may be present in many compounds.

Methods.—We purchased samples from MTI Corp.: CdS single crystal, (0001) orientation; ZnS polycrystal, multi-spectral grade; ZnO single crystal, (1120) orientation (a-plane). We measured samples as-received and after annealing at 500 °C for 120 h in a vacuum atmosphere

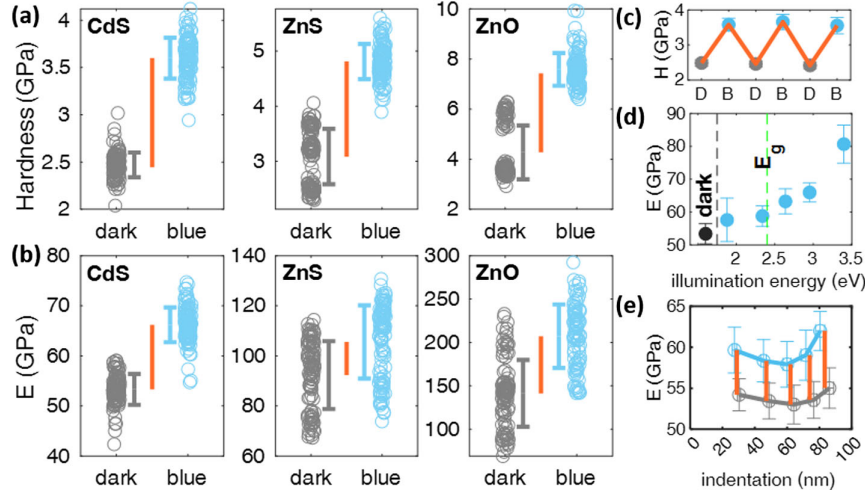


FIG. 1. Giant optomechanical effects in wide-band-gap II-VI compounds measured by nanoindentation. (a) Hardness and (b) Young's modulus (E) measured in the dark and under blue illumination by an LED with center wavelength 470 nm; irradiance at the sample surface is 1.4 mW/cm^2 . The data shown include three successive cycles of darkness or illumination, and at each condition the measurement is repeated at 36 distinct locations, for a total of 108 separate measurements each for dark and illuminated conditions. The individual data are plotted directly; errorbars report average and standard deviation. Orange bars indicate the average change between dark and illuminated conditions. (c)–(e) Additional details provided for measurements on CdS. (c) Hardness during successive conditions of dark (D) and blue illumination (B). The data and error bars report the average and standard deviation of the 36 measurements performed at each condition; orange line traces the averages. (d) Dependence of E on the color of illumination, from red to uv; result of measurements in the dark are also shown. The irradiance is different for each condition: red (660 nm, 1.9 eV) = 3.3 mW/cm^2 ; green (530 nm, 2.3 eV) = 0.99 mW/cm^2 ; blue (470 nm, 2.6 eV) = 1.4 mW/cm^2 ; violet (420 nm, 3.0 eV) = 1.9 mW/cm^2 ; uv (365 nm, 3.4 eV) = 22 mW/cm^2 . (e) Depth dependence of the photoelastic effect, showing dark conditions (gray) and blue illumination (blue); illumination conditions are as in (a)–(c). Error bars on individual points represent the standard deviation of repeated measurements, and the solid lines are guides to the eye. The orange vertical bars indicate the photoelastic effect.

(CdS, ZnS, and ZnO, “ann. 1” below) and in a sulfur atmosphere (CdS and ZnS, “ann. 2” below). All samples were measured with as-delivered surfaces except for the vacuum-annealed ZnO, which we polished before measurement. We obtained a sample of ZnO with record-low defect density, made by homoepitaxial growth (film thickness 800 nm) with ozone-assisted molecular beam epitaxy [24]. We performed nanoindentation measurements using a Bruker Hysitron TriboIndenter 950, equipped with a standard diamond Berkovich tip. We performed measurements in two modes, high-speed indentation, and depth profiling. We illuminated samples during indentation using a custom-built illuminator.

We use DFT to study the contribution of point defect ionization and subsequent lattice relaxation to photoelasticity [25,26]. We simulate $2 \times 2 \times 2$, $2 \times 2 \times 3$, and $3 \times 3 \times 2$ CdS supercells with one sulfur atom removed in each case, corresponding to vacancy concentrations 6.25%, 4.17%, and 2.78%, respectively. An uncharged supercell, with no electrons removed, corresponds to a neutral vacancy (V_S^\times), whereas a supercell with two electrons removed corresponds to a doubly ionized vacancy (V_S^{2+}).

Results.—We find large and reversible photo hardening of CdS, ZnS, and ZnO. In Figs. 1(a) and 1(b) we present the hardness and Young's modulus (E) measured by

nanoindentation in the dark and under blue illumination (470 nm, 1.4 mW/cm^2). Each dataset for a given illumination condition represents measurements at 108 distinct locations on the sample surface during successive cycles of light and dark conditions. In Fig. 1(c) we show the history dependence of hardness measured on CdS through multiple illumination cycles. CdS shows the largest and most repeatable optomechanical response. ZnS shows photohardening, but much smaller photo-elasticity than CdS. This is expected if sulfur vacancies are the source of giant photoelasticity, because multispectral ZnS is treated to improve optical transparency by reducing the sulfur vacancy concentration. However, despite the substantial dispersion in the measured data for ZnS, there is greater than 99% confidence that the dark and illuminated conditions have different elastic modulus (Student's $|t| = 6.6$). ZnO shows sizable photohardening and photoelasticity, but also shows the largest memory effect.

We find that the optomechanical effects increase as the illumination energy increases towards the band gap for all samples. In Fig. 1(d) we show the dependence of E measured on CdS with varying illumination wavelength: the photoelastic effect is finite but small for below-band gap light, then increases quickly for blue, violet, and uv illumination. This is evidence that the optomechanical

response is associated with carrier generation and trapping at defect levels. Depth-profile measurements reveal a non-monotonic depth dependence of the photoelastic effect [Fig. 1(e)]. The effect is enhanced at larger indentation depth, which could result from interaction between charge trapping at point defects and an increasing concentration of dislocations, which may themselves be light sensitive, as are some screw dislocations in CdS [27]. Depth dependence may arise from interplay of nanoindentation geometry with nonisotropic photoelasticity. We also see a slight enhancement of photostiffening near the sample surface, which could result from stronger near-surface light absorption.

It is established that photoplasticity is related to photoconductivity by the interaction of dislocations with charge trapped at point defects [4,5]. Ionization of point defects associated with persistent photoconductivity is accompanied by substantial lattice relaxation; this was described for III-V semiconductors by Lang and Logan, later for ZnO, CuInSe₂, and CuGaSe₂ by Zhang, Wei, Zunger, and Lany, and more recently for CdS by ourselves [19,21–23]. These patterns of lattice relaxations create energy barriers that forestall carrier capture and recombination, so that photoexcitation produces persistent photoexcited ionized states. The effects of such lattice relaxations on elastic properties have not been studied, to our knowledge. We hypothesize that charge trapping at point defects under illumination is responsible for both photoplasticity and photoelasticity. To test this hypothesis, we anneal our samples to change point defect concentrations. We present our results in Fig. 2. We find that annealing reduces the photoplastic and photoelastic effects in all samples. These results confirm that the photoelastic effect can be controlled by materials processing, but do not yet directly confirm our hypothesis, because the defect concentrations remain unknown. Inductively coupled plasma optical emission spectroscopy (ICP-OES) measurements on CdS find an increase in S/Cd ratio upon annealing, changing from 0.958 ± 0.006 for the original sample, to 0.980 ± 0.001 and 0.976 ± 0.002 for the vacuum- and sulfur-annealed samples, respectively (error bars represent the statistical deviation of multiple measurements), consistent with our hypothesis. ICP-OES cannot measure intrinsic defect concentrations in ZnS and ZnO. As a further test, we measured the optomechanical response of homoepitaxial ZnO with record-low defect density [24]. We find that this nearly perfect ZnO has no optomechanical response, further supporting our hypothesis that photoplasticity and photoelasticity results from charge state transitions at point defects.

Next, we evaluate theoretical models to explain giant photoelasticity. We find that the local effects of lattice relaxation around ionized point defects are semiquantitatively consistent with the experimental observations. More conventional models of photostriction and the piezoelectric effect are not consistent with experiments.

We focus first on CdS, for which it is understood that charge trapping and lattice relaxation at sulfur vacancies is

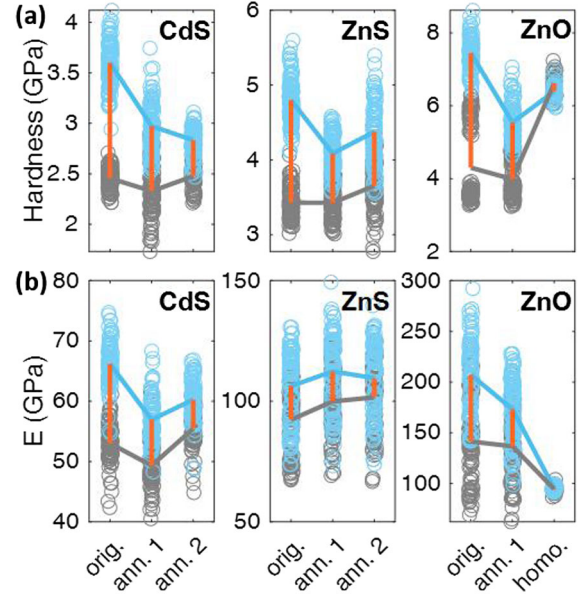


FIG. 2. Controlling giant optomechanical effects through sample processing. (a) Hardness and (b) Young's modulus (E) measured in the dark and under illumination by an LED for samples processed with different annealing conditions. Illumination conditions are the same as in Fig. 1. Gray and blue symbols indicate individual measurements taken during three successive dark or illumination cycles, totaling 108 separate measurements for each condition. Gray and blue lines trace the average for each condition, and the orange bars highlight the change upon illumination. The samples are labeled “orig.” for the original, as-received samples, “ann. 1” for vacuum-annealed samples, “ann. 2” for sulfur-annealed samples, and “homo.” for homoepitaxial ZnO.

responsible for persistent photoconductivity [23]. Sulfur vacancies are deep double donors occupied by two electrons at equilibrium (V_S^\times in Kroger-Vink notation). Upon ionization, the lattice relaxes around the vacancy so as to raise the transition energy level close to the conduction band edge, converting the defect into a shallow donor; we have termed this defect-level switching [28]. In Figs. 3(a) and 3(b) we illustrate how the atomic lattice changes, first upon introduction of a neutral vacancy (V_S^\times), and then by vacancy ionization ($V_S^\times \rightarrow V_S^{\bullet}$). Upon introducing V_S^\times we observe a peculiar pattern of lattice relaxation, whereby three of the Cd ions move inwards towards the vacancy, while one moves out [Fig 3(a)]. This three-in, one-out pattern can be reproduced with any one of three Cd ions directed mainly in the \hat{a} - \hat{b} plane from the sulfur vacancy moving outward. However, the forth, directed along \hat{c} , cannot be made to relax outward. Even manually initiating the energy minimization with this forth ion displaced downward (in the view in Fig. 3) results in its relaxation inward, and the selection of a different ion to relax outward. For a simpler case we also model cubic ZnS. In Figs. 3(c) and 3(d) we illustrate the same sequence from the pristine lattice, to a neutral vacancy (V_S^\times), to an ionized vacancy

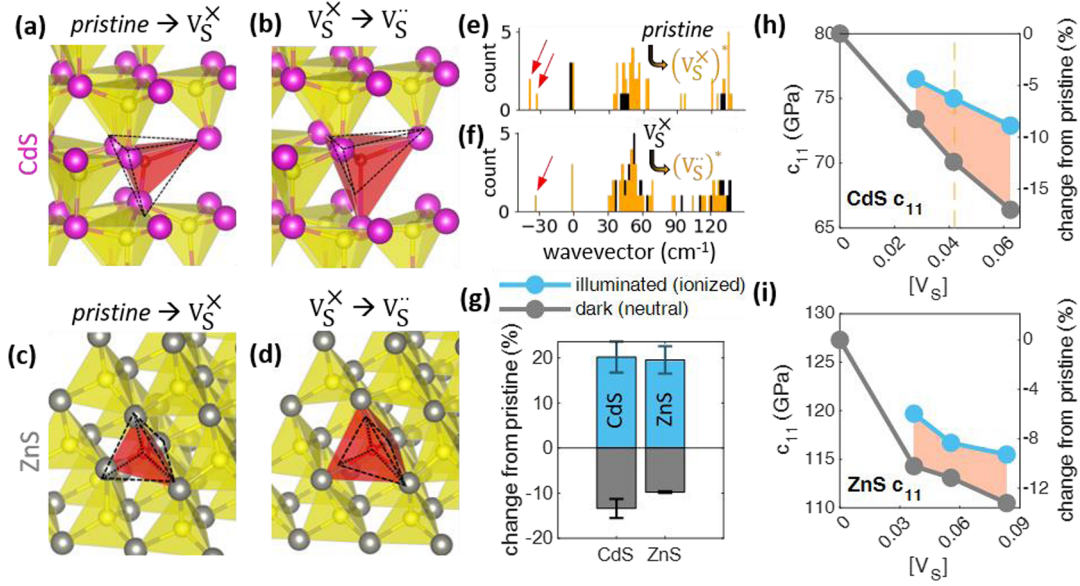


FIG. 3. Theoretical results for the change in the crystal lattice and elastic properties upon sulfur vacancy double ionization in CdS and ZnS. (a)–(b) Visualizing the lattice changes in CdS through the sequence: $\text{pristine} \rightarrow V_S^X \rightarrow V_S^{\bullet\bullet}$. Cd atoms shown in magenta, S shown in yellow; the missing sulfur atom and its coordination polyhedron are shown in red. (a) Change upon introducing a neutral sulfur vacancy. Black dashed line traces the Cd_4 tetrahedron in the pristine lattice, red polyhedron highlights the Cd_4 arrangement after introducing the vacancy and relaxing the lattice. (b) Change upon ionizing the sulfur vacancy. Black dashed line traces the Cd_4 tetrahedron in the lattice with neutral V_S^X , red polyhedron highlights the Cd_4 arrangement after ionizing and relaxing the lattice. (c)–(d) As in (a)–(b), but for the case of ZnS; Zn atoms are shown in gray. (e)–(f) Γ -point phonon DOS presented as histograms; negative-frequency modes that drive lattice relaxation are indicated with red arrows. (e) Data for pristine CdS, and after creating a sulfur vacancy but before relaxing the lattice [indicated as excited state $(V_S^X)^*$]. (f) Data for a relaxed lattice with a neutral vacancy, and after ionizing the vacancy but before relaxing the lattice [indicated as excited state $(V_S^{\bullet\bullet})^*$]. (g) Change in Cd-Cd and Zn-Zn distances around a sulfur vacancy, relative to the pristine lattice. Distances contract around V_S^X and expand around $V_S^{\bullet\bullet}$, as illustrated in (a)–(d). Error bars present the span of results calculated for varying $[V_S]$, up to 6.25% and 8.33% missing sulfur atoms for the case of CdS and ZnS, respectively. (h) Change in c_{11} for neutral and doubly ionized vacancies in CdS, for a range of missing sulfur atoms fractions $[V_S]$. The photoelastic response is the difference between the neutral (gray, representing dark conditions) and ionized (blue, representing illuminated conditions) data, colored in orange. The orange dashed line marks $[V_S]$ for the original CdS sample, determined by ICP-OES. (i) As in (h), but for the case of ZnS.

($V_S^{\bullet\bullet}$). We again observe a pattern of broken rotational symmetry around V_S^X , with one Zn ion protruding. However, due to the higher symmetry of ZnS *vis-à-vis* CdS, any of the four Zn ions can be selected to protrude. These details pose interesting questions about how the three-in, one-out pattern manifests in real samples.

For a complementary view of the lattice instabilities and relaxation pathways, we analyze the phonon spectra. In Figs. 3(e) and 3(f) we present the zone center (Γ point) phonon density of states (DOS) of CdS in four cases, calculated from a $2 \times 2 \times 2$ supercell. In Fig. 3(e) we plot the spectra for a pristine lattice, and for the lattice after introducing a V_S^X site but before relaxation. The negative-frequency phonon modes signal the lattice instability. We observe two negative-frequency branches: a single mode at -33 cm^{-1} corresponding to an outward relaxation of the Cd ion directed along \hat{c} , and a degenerate mode at -39 cm^{-1} corresponding to outward relaxation of one of the other three Cd ions. This frequency splitting explains the observation, in our numerical experiments, that the

three-in, one-out pattern always selects one of the three Cd ions mainly in the \hat{a} - \hat{b} plane, but never the one directed along \hat{c} . The modes at -39 cm^{-1} correspond closely to the relaxation illustrated in Fig. 3(a).

In Fig. 3(f) we plot the spectra for a relaxed lattice with a V_S^X site, and for the lattice after ionizing but before relaxation. We observe one negative-frequency branch, which corresponds to the outward relaxation illustrated in Fig. 3(b). In this case there is no degeneracy, because the three-in, one-out pattern is already selected at the start of the simulation.

$V_S^X \rightarrow V_S^{\bullet\bullet}$ ionization is accompanied by a large lattice relaxation in both CdS and ZnS. In Fig. 3(g) we quantify the change in Cd-Cd and Zn-Zn spacing relative to the pristine lattice, and we see that cation-cation distances change by more than 30% upon ionization. Because of these large lattice relaxations, the ionized state is metastable, with relaxation times on the order of 1 s or longer at room temperature for CdS. As a result even mild illumination can maintain a high fraction of defect ionization [23].

The large lattice relaxations are accompanied by large changes in the elasticity. In Figs. 3(h) and 3(i) we present the calculated c_{11} for varying $[V_S]$ for CdS and ZnS for the cases of neutral and ionized vacancies. Although introducing vacancies softens the lattice relative to the pristine case, the lattice then stiffens upon ionization $V_S^\times \rightarrow V_S^{\bullet\bullet}$: this is the photoelastic effect. DFT predicts a large photoelastic effect, on the order of 5% for the realistic $[V_S]$.

Summary.—We establish that giant photoelasticity is a generic phenomenon in common wide-band-gap compound semiconductors, and we show that both photoelasticity and photoplasticity can be tuned by materials processing. We demonstrate that the phenomena of ionization and lattice relaxation at point defects have substantial impacts on material elastic properties, far larger than the effects of photostriction and piezoelectricity. In the Supplemental Material we describe further the methods used, and present additional results and analysis [29–49].

Our results suggest future research into applications of giant optomechanics for structural metals, flexible electronics, and radiofrequency filters. We also anticipate further fundamental research into the nanomechanical properties of point defect transformations, including in lesser-studied semiconductors and in layered materials with highly anisotropic mechanical properties. There is an opportunity to advance DFT methods to more accurately model the elastic properties of crystals with neutral and ionized point defects. Orbital physics could help to explain trends in lattice relaxation; for instance, the three-in, one-out pattern observed here could result from a Jahn-Teller effect acting on cation molecular orbitals. There is also an open question of how the pattern of broken symmetry manifests across a population of defects. We hypothesize that long-range stress and strain fields can mediate interactions between the configurations of distant defects, producing an elastic tensor with symmetry distinct from the pristine crystal. Fields introduced during mechanical testing could similarly interact with point defect configurations, making the elastic tensor a dynamical field that interacts with both illumination and applied stress.

We acknowledge Brian Neltner, David Bono, Austin Akey, and Aubrey Penn for technical assistance. We acknowledge Joseph Falson and Masashi Kawasaki for providing a sample for study. We acknowledge illuminating discussion with Alexandru Georgescu. This work was supported by the Office of Naval Research MURI through Grant No. N00014-17-1-2661. We acknowledge use of the NanoMechanical Technology Laboratory in the Department of Materials Science and Engineering at MIT.

*These authors contributed equally to this work.

†rjaramil@mit.edu

[1] T. Figielski, Photostriction effect in germanium, *Phys. Status Solidi* **1**, 306 (1961).

- [2] M. H. Zhao, Z.-Z. Ye, and S. X. Mao, Photoinduced Stiffening in ZnO Nanobelts, *Phys. Rev. Lett.* **102**, 045502 (2009).
- [3] J. T. Lin, P. D. Shuvra, S. McNamara, H. Gong, W. Liao, J. L. Davidson, K. M. Walsh, M. L. Alles, and B. W. Alphenaar, Near-Surface Electronic Contribution to Semiconductor Elasticity, *Phys. Rev. Applied* **8**, 034013 (2017).
- [4] Yu. A. Osip'yan and V. F. Petrenko, Nature of the photoplastic effect, *Sov. J. Exp. Theor. Phys.* **36**, 916 (1973).
- [5] V. F. Petrenko and R. W. Whitworth, Charged dislocations and the plastic-deformation of II-VI compounds, *Philos. Mag. A* **41**, 681 (1980).
- [6] Y. Osipyan, V. Petrenko, A. Zaretskii, and R. Whitworth, Properties of II-VI semiconductors associated with moving dislocations, *Adv. Phys.* **35**, 115 (1986).
- [7] T. Garosshen, C. Kim, and J. Galligan, On the influence of light on dislocation-motion in compound semiconductors, *J. Electron. Mater.* **19**, 889 (1990).
- [8] L. Carlsson, Orientation and temperature dependence of the photoplastic effect in ZnO, *J. Appl. Phys.* **42**, 676 (1971).
- [9] L. Carlsson and C. Svensson, Photoplastic effect in ZnO, *J. Appl. Phys.* **41**, 1652 (1970).
- [10] R. H. Bube, *Photoconductivity of Solids* (Wiley, New York, 1960).
- [11] B. Wolf, A. Belger, D. C. Meyer, and P. Paufler, On the impact of light on nanoindentations in ZnSe, *Phys. Status Solidi A* **187**, 415 (2001).
- [12] B. Wolf and A. Richter, The concept of differential hardness in depth sensing indentation, *New J. Phys.* **5**, 15 (2003).
- [13] X. J. Zheng, G. C. Yu, Y. Q. Chen, S. X. Mao, and T. Zhang, Photoinduced stiffening and photoplastic effect of ZnS individual nanobelt in nanoindentation, *J. Appl. Phys.* **108**, 094305 (2010).
- [14] Y. Wei, L. H. Xu, Y. W. Tao, X. J. Zheng, J. H. Yang, D. F. Zou, and S. X. Mao, Width-to-thickness ratio dependence on photoplastic effect of ZnS nanobelt, *Appl. Phys. Lett.* **101**, 091904 (2012).
- [15] Y. Oshima, A. Nakamura, and K. Matsunaga, Extraordinary plasticity of an inorganic semiconductor in darkness, *Science* **360**, 772 (2018).
- [16] K. Tanaka, N. Kawakami, and A. Odajima, Photoinduced elastic changes in amorphous As₂S₃ films, *Jpn. J. Appl. Phys.* **20**, L874 (1981).
- [17] K. Tanaka, Reversible photostructural change: Mechanisms, properties and applications, *J. Non-Cryst. Solids* **35–36**, 1023 (1980).
- [18] J. Lagowski and H. C. Gatos, Photomechanical effect in noncentrosymmetric semiconductors—CdS, *Appl. Phys. Lett.* **20**, 14 (1972).
- [19] D. V. Lang and R. A. Logan, Large-Lattice-Relaxation Model for Persistent Photoconductivity in Compound Semiconductors, *Phys. Rev. Lett.* **39**, 635 (1977).
- [20] P. M. Mooney, Deep donor levels (DX Centers) in III-V semiconductors, *J. Appl. Phys.* **67**, R1 (1990).
- [21] S. B. Zhang, S.-H. Wei, and A. Zunger, Intrinsic N-type versus p-type doping asymmetry and the defect physics of ZnO, *Phys. Rev. B* **63**, 075205 (2001).
- [22] S. Lany and A. Zunger, Anion vacancies as a source of persistent photoconductivity in II-VI and chalcopyrite semiconductors, *Phys. Rev. B* **72**, 035215 (2005).

- [23] H. Yin, A. Akey, and R. Jaramillo, Large and persistent photoconductivity due to hole-hole correlation in CdS, *Phys. Rev. Mater.* **2**, 084602 (2018).
- [24] J. Falson, Y. Kozuka, M. Uchida, J. H. Smet, T. Arima, A. Tsukazaki, and M. Kawasaki, MgZnO/ZnO heterostructures with electron mobility exceeding 1×10^6 Cm²/Vs, *Sci. Rep.* **6**, 26598 (2016).
- [25] G. Kresse and J. Furthmüller, Efficient iterative schemes for Ab Initio total-energy calculations using a plane-wave basis set, *Phys. Rev. B* **54**, 11169 (1996).
- [26] G. Kresse and J. Furthmüller, Efficiency of Ab-Initio total energy calculations for metals and semiconductors using a plane-wave basis set, *Comput. Mater. Sci.* **6**, 15 (1996).
- [27] A. A. Istratov and O. F. Vyvenko, DX-like center generated by uniaxial strains of screw dislocations in CdS, *J. Appl. Phys.* **80**, 4400 (1996).
- [28] H. Yin, A. Kumar, J. M. LeBeau, and R. Jaramillo, Defect-Level Switching for Highly Nonlinear and Hysteretic Electronic Devices, *Phys. Rev. Applied* **15**, 014014 (2021).
- [29] A. C. Fischer-Cripps, *Nanoindentation*, 2nd ed. (Springer-Verlag, New York, 2004).
- [30] W. Kohn and L. J. Sham, Self-consistent equations including exchange and correlation effects, *Phys. Rev.* **140**, A1133 (1965).
- [31] P. Hohenberg and W. Kohn, Inhomogeneous electron gas, *Phys. Rev.* **136**, B864 (1964).
- [32] J. P. Perdew, K. Burke, and M. Ernzerhof, Generalized Gradient Approximation Made Simple, *Phys. Rev. Lett.* **77**, 3865 (1996).
- [33] Y. Le Page and P. Saxe, Symmetry-general least-squares extraction of elastic data for strained materials from Ab Initio calculations of stress, *Phys. Rev. B* **65**, 104104 (2002).
- [34] X. Wu, D. Vanderbilt, and D. R. Hamann, Systematic treatment of displacements, strains, and electric fields in density-functional perturbation theory, *Phys. Rev. B* **72**, 035105 (2005).
- [35] G. Makov and M. C. Payne, Periodic boundary conditions in Ab Initio calculations, *Phys. Rev. B* **51**, 4014 (1995).
- [36] J. Neugebauer and M. Scheffler, Adsorbate-substrate and adsorbate-adsorbate interactions of Na and K adlayers on Al(111), *Phys. Rev. B* **46**, 16067 (1992).
- [37] A. Walsh, Correcting the corrections for charged defects in crystals, *npj Comput. Mater.* **7**, 72 (2021).
- [38] P. Giannozzi *et al.*, QUANTUM ESPRESSO: A modular and open-source software project for quantum simulations of materials, *J. Phys. Condens. Matter* **21**, 395502 (2009).
- [39] P. Giannozzi *et al.*, Advanced capabilities for materials modelling with quantum ESPRESSO, *J. Phys. Condens. Matter* **29**, 465901 (2017).
- [40] A. Kokalj, XCrySDen—A new program for displaying crystalline structures and electron densities, *J. Mol. Graphics Modell.* **17**, 176 (1999).
- [41] X. Fu *et al.*, Tailoring exciton dynamics by elastic strain-gradient in semiconductors, *Adv. Mater.* **26**, 2572 (2014).
- [42] K. Nishidate, T. Sato, Y. Matsukura, M. Baba, M. Hasegawa, and T. Sasaki, Density-functional electronic structure calculations for native defects and Cu impurities in CdS, *Phys. Rev. B* **74**, 035210 (2006).
- [43] H. H. Woodbury, Diffusion of Cd in CdS, *Phys. Rev.* **134**, A492 (1964).
- [44] J. S. McCloy, W. Wolf, E. Wimmer, and B. J. Zelinski, Impact of hydrogen and oxygen defects on the lattice parameter of chemical vapor deposited zinc sulfide, *J. Appl. Phys.* **113**, 023706 (2013).
- [45] N. Hernandez-Como, V. Martinez-Landeros, I. Mejia, F. S. Aguirre-Tostado, C. D. Nascimento, G. de M. Azevedo, C. Krug, and M. A. Quevedo-Lopez, Defect control in room temperature deposited cadmium sulfide thin films by pulsed laser deposition, *Thin Solid Films* **550**, 665 (2014).
- [46] L. J. Brillson, Surface photovoltage and auger spectroscopy studies of (11 $\bar{2}$ 0) CdS surface, *J. Vac. Sci. Technol.* **12**, 249 (1975).
- [47] S. Simov, M. Kalitzova, E. Nikolova, and I. Baltov, Surface photovoltage spectroscopy study of CdS thin films, *Surface Sci.* **59**, 115 (1976).
- [48] D. Berlincourt, H. Jaffe, and L. R. Shiozawa, Electroelastic properties of the sulfides, selenides, and tellurides of zinc and cadmium, *Phys. Rev.* **129**, 1009 (1963).
- [49] See Supplemental Material at <http://link.aps.org/supplemental/10.1103/PhysRevLett.129.065501> for further details on the methods used, and additional results and analysis.